Supplementary information

Effect of biphenyl groups on the properties of poly(fluorenylidene piperidinium) based anion exchange membranes for applications to water electrolyzers

Ahmed Mohamed Ahmed Mahmoud,[1,2] Kenji Miyatake,[1,3,4] Fanghua Liu,[1] Vikrant Yadav,[1] Fang Xian,[1] Lin Guo,[1] Chun Yik Wong,[1] Toshio Iwataki,[3] Makoto Uchida,[3] Katsuyoshi Kakinuma[1,3]*

1. Clean Energy Research Center, University of Yamanashi, Kofu, 400-8510, Japan.

2. Chemistry Department, Faculty of Science, Sohag University, Sohag, 82524, Egypt

3. Hydrogen and Fuel Cell Nanomaterials Center, University of Yamanashi, Kofu, 400-8510, Japan.

4. Department of Applied Chemistry, Waseda University, Tokyo, 169-8555, Japan.

*: Corresponding author
E-mail: miyatake@yamanashi.ac.jp

Figures and Tables

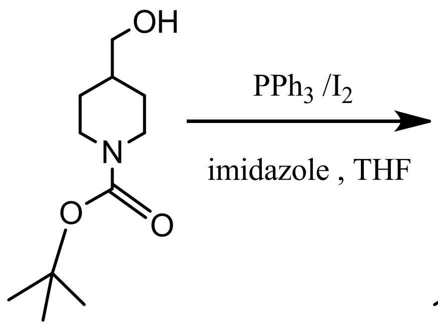

Scheme S1 Synthesis of tert-butyl-4-(iodomethyl)piperidine-1-carboxylate.

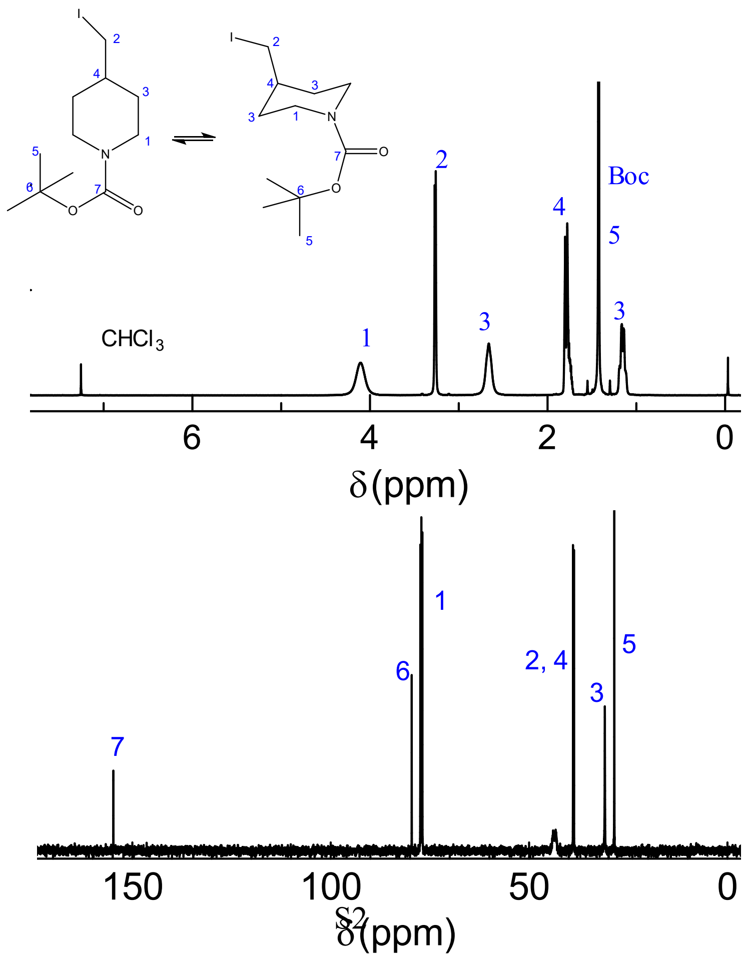

Fig. S1 ^{1}H and ^{13}C NMR spectra of *tert*-butyl 4-(iodomethyl)piperidine-1-carboxylate.

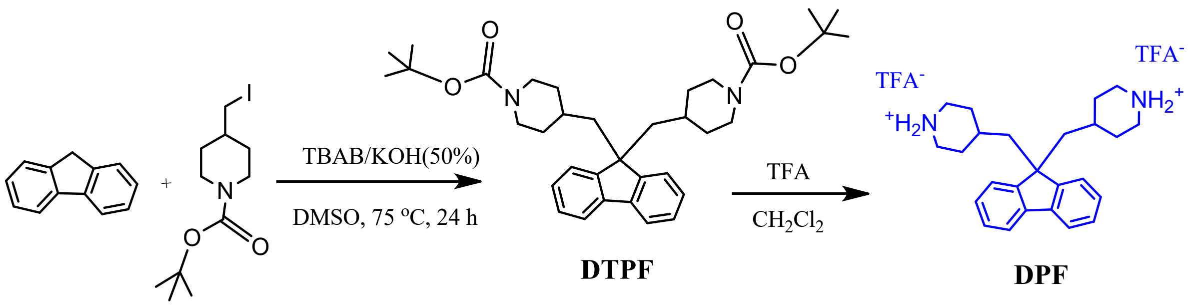

Scheme S2 Synthesis of 4,4'-((9H-fluorene-9,9-diyl)bis(methylene))bis(piperidin-1-ium)trifluoroacetate (DPF).

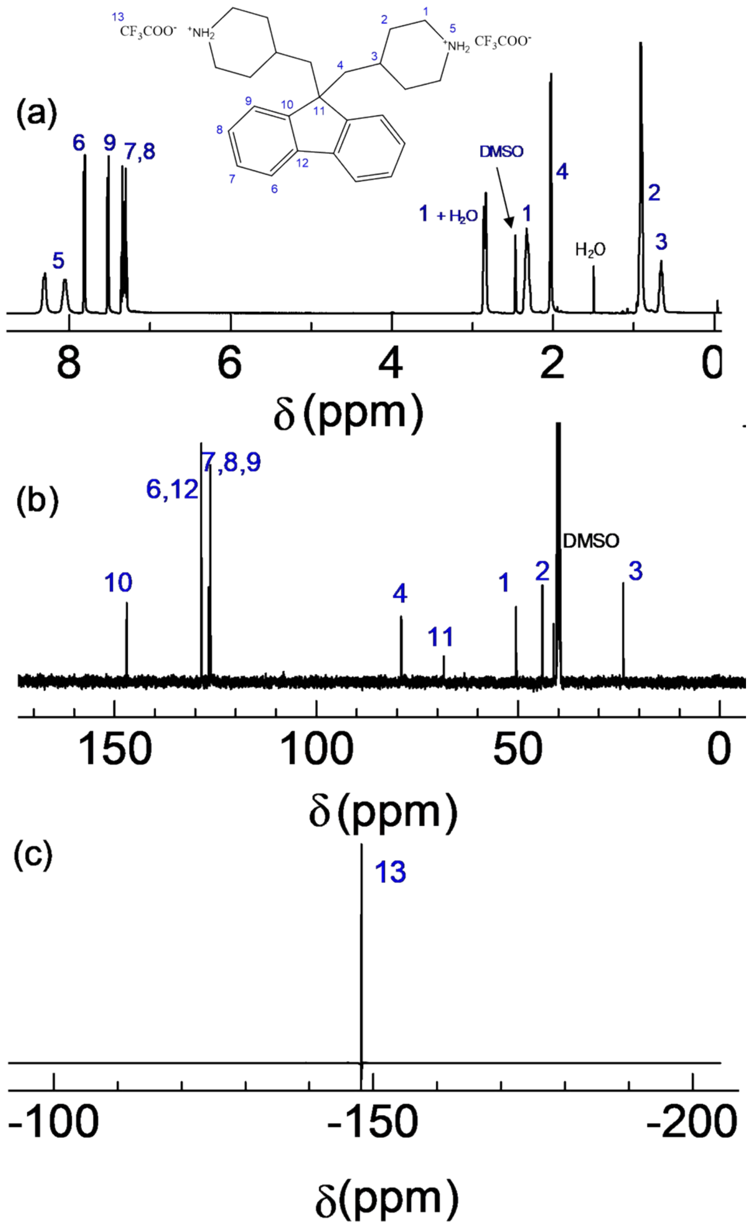

Fig. S2 (a) ^1H, (b) ^{13}C, and (c) ^{19}F NMR spectra of 4,4'-((9*H*-fluorene-9,9-diyl)bis(methylene))bis(piperidin-1-ium)trifluoroacetate (DPF).

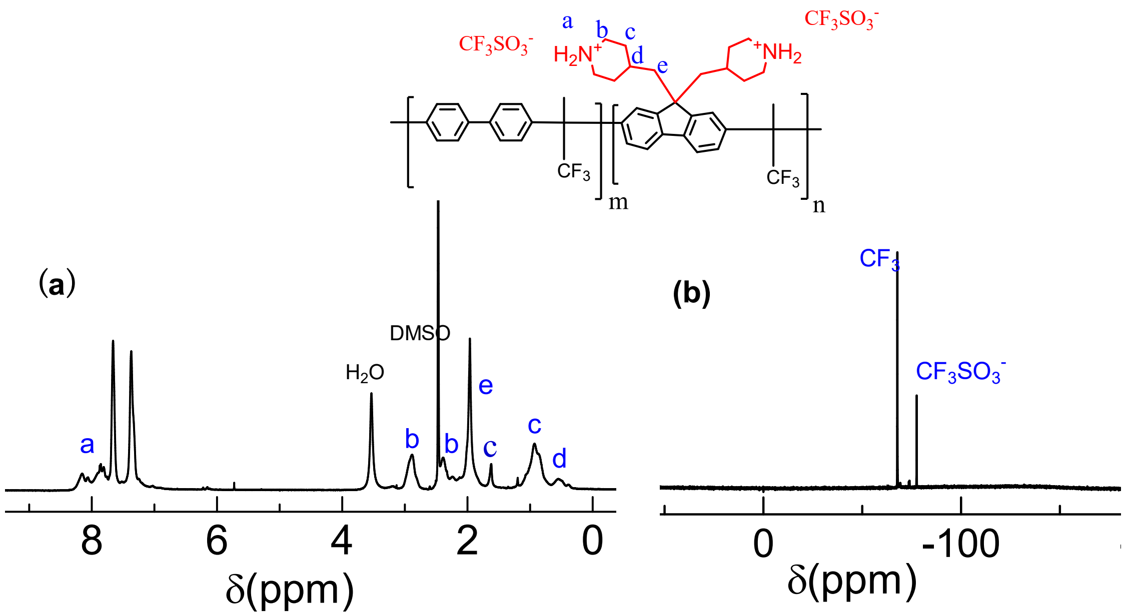

Fig. S3 (a) ^{1}H and (b) ^{19}F NMR spectra of protonated BPh-Pip copolymer.

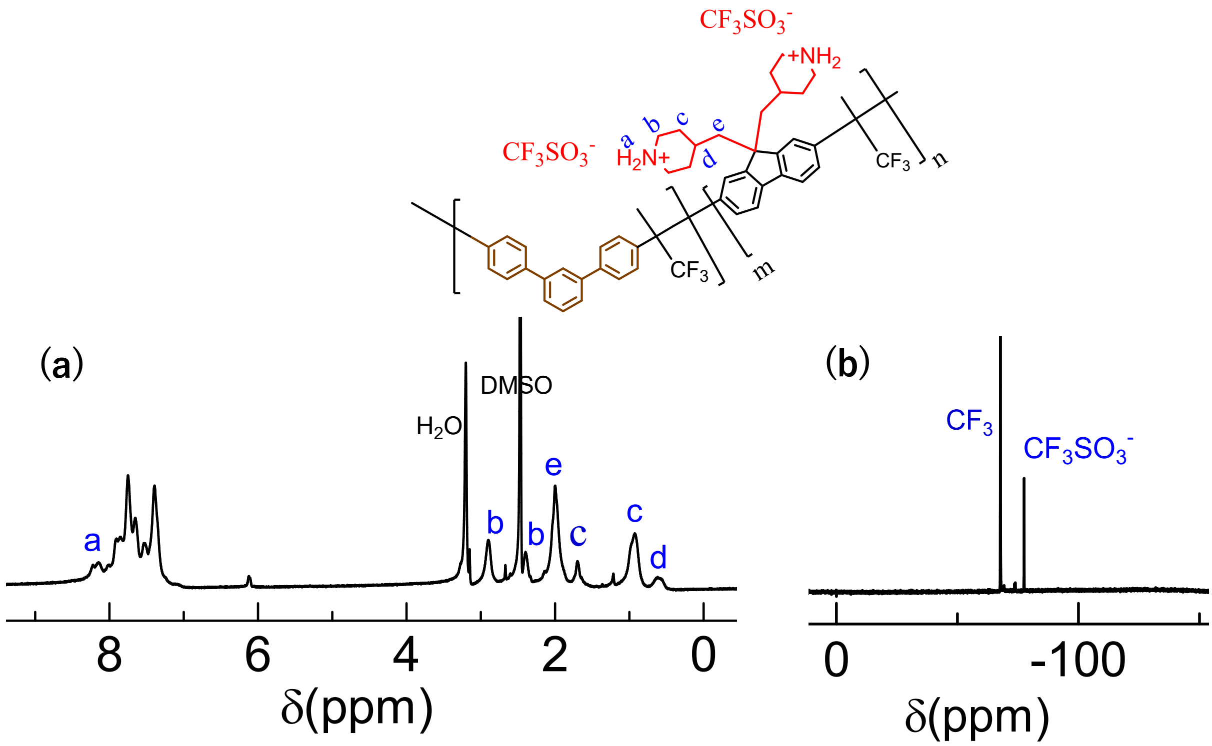

Fig. S4 (a) ^1H and (b) ^{19}F NMR spectra of mTPh-Pip copolymer.

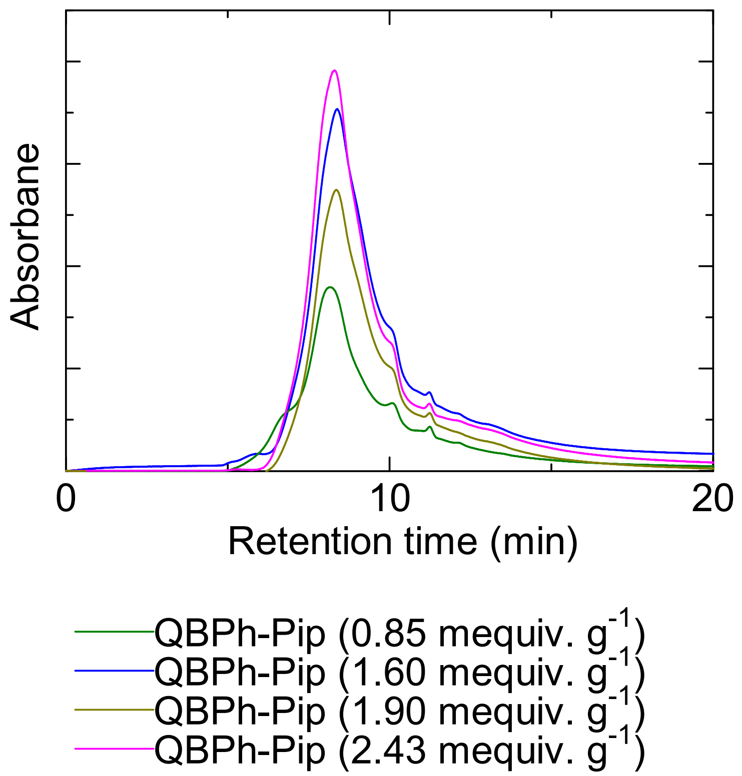

Fig. S5 GPC profiles of QBPh-Pip copolymers.

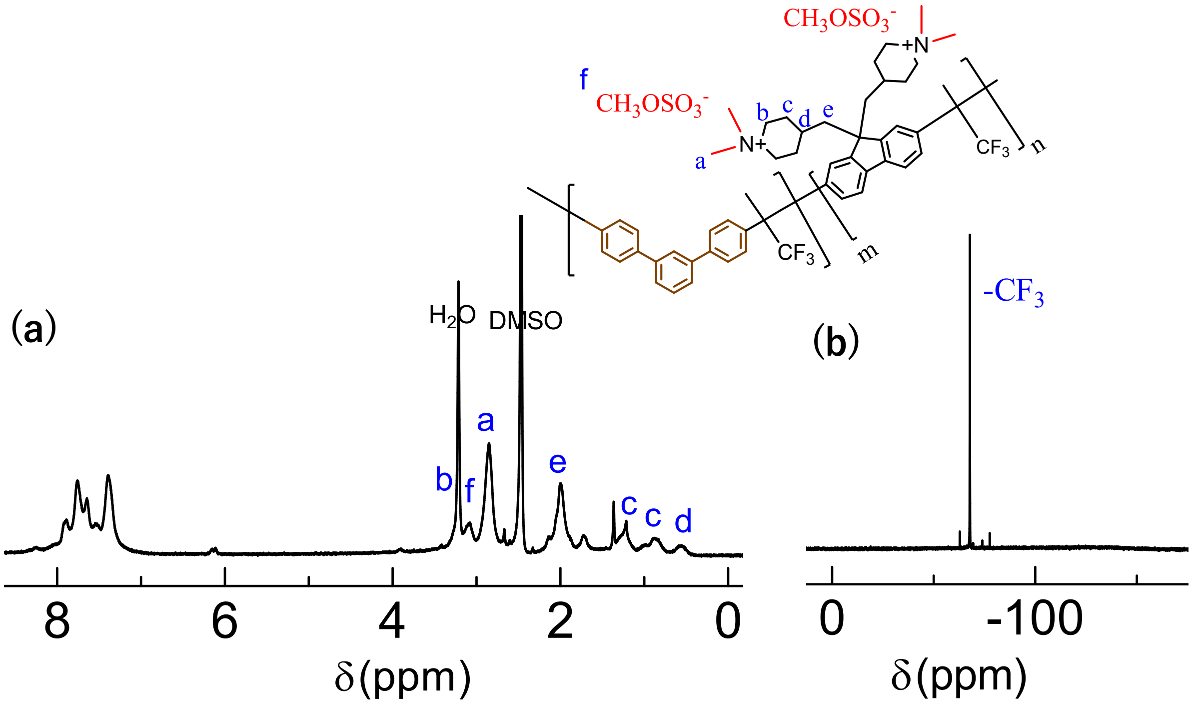

Fig. S6 (a) ^{1}H and (b) ^{19}F NMR spectra of QmTPh-Pip copolymer (target IEC = 2.0 mequiv. g^{-1}).

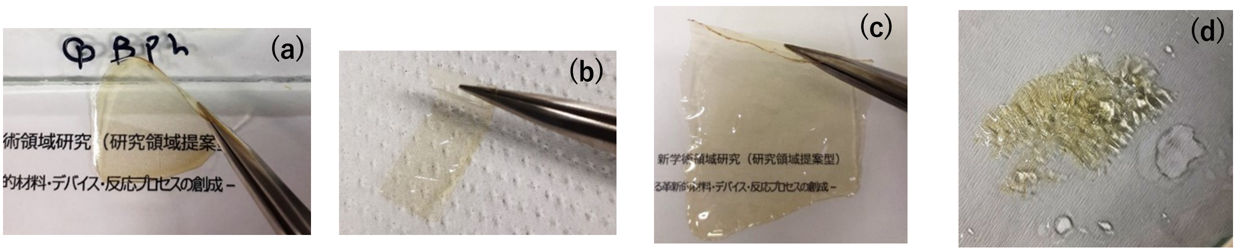

IEC_{tit} = 0.80 mequiv. g^{-1} IEC_{tit} = 1.60 mequiv. g^{-1} IEC_{tit} = 1.90 mequiv. g^{-1} IEC_{tit} = 2.43 mequiv. g^{-1}

Fig. S7 (a,b,c) Photos of dry QBPh-Pip membranes with different IECs. (d) after contact with water drops at room temperature.

IEC_{tit} = 0.78 mequiv. g^{-1} IEC_{tit} = 1.52 mequiv. g^{-1} IEC_{tit} = 1.96 mequiv. g^{-1}

Fig. S8 Photos of cracked QmTPh-Pip membranes.

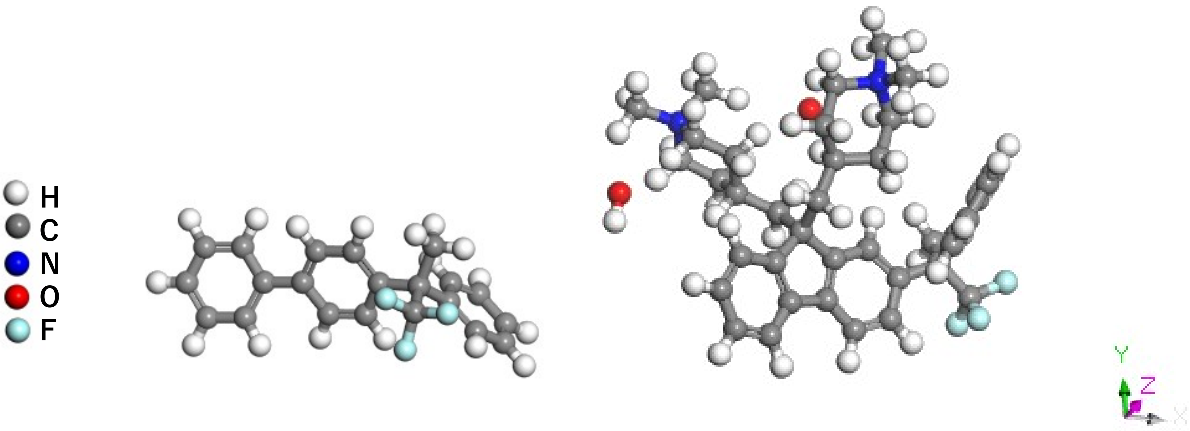

Hydrophobic component Hydrophilic component

Occupied volume: 268.2 Å ^{3} **Occupied volume : 666.4 Å ^{3}**

Fig. S9 Molecular volume of the hydrophilic and hydrophobic components of QBPh-Pip estimated from DFT calculations using Dmol^3 software.

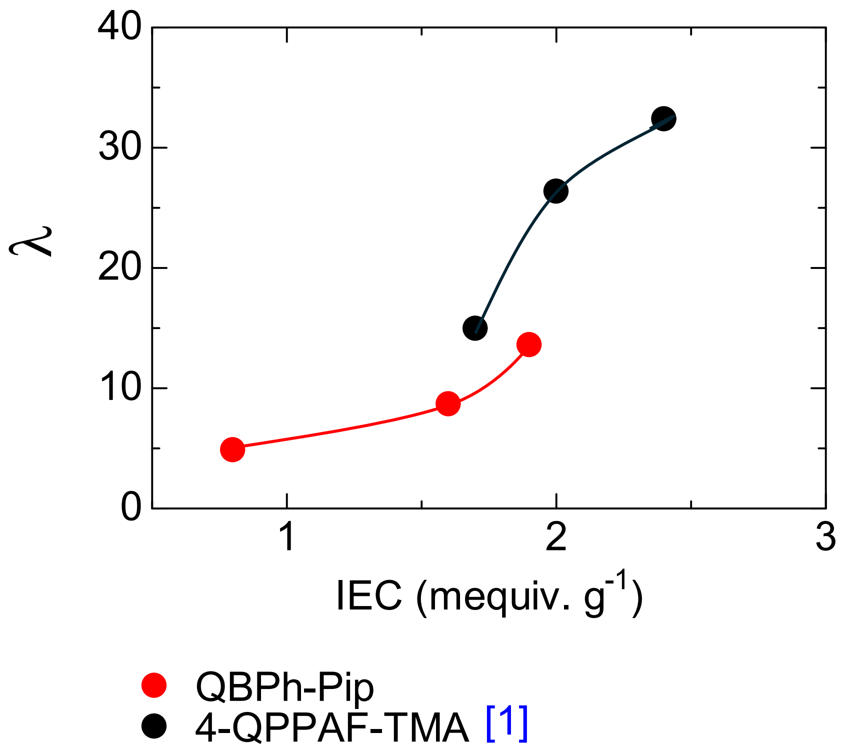

Fig. S10 Number of water molecules per ammonium group (λ) at 30 °C of QBPh-Pip and 4-QPPAF-TMA [adapted from ref 1] as a function of IEC.

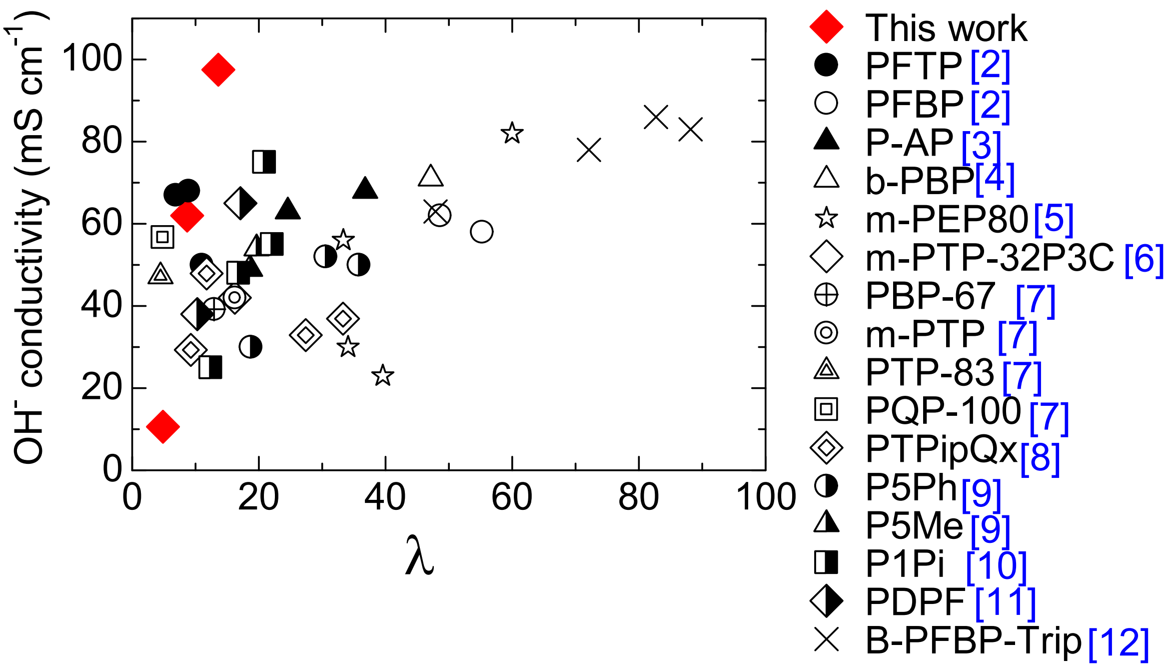

Fig. S11 Hydroxide ion conductivity of QBPh-Pip and some other reported AEMs as a function of number of water molecules per ammonium group (λ) at 30 °C.

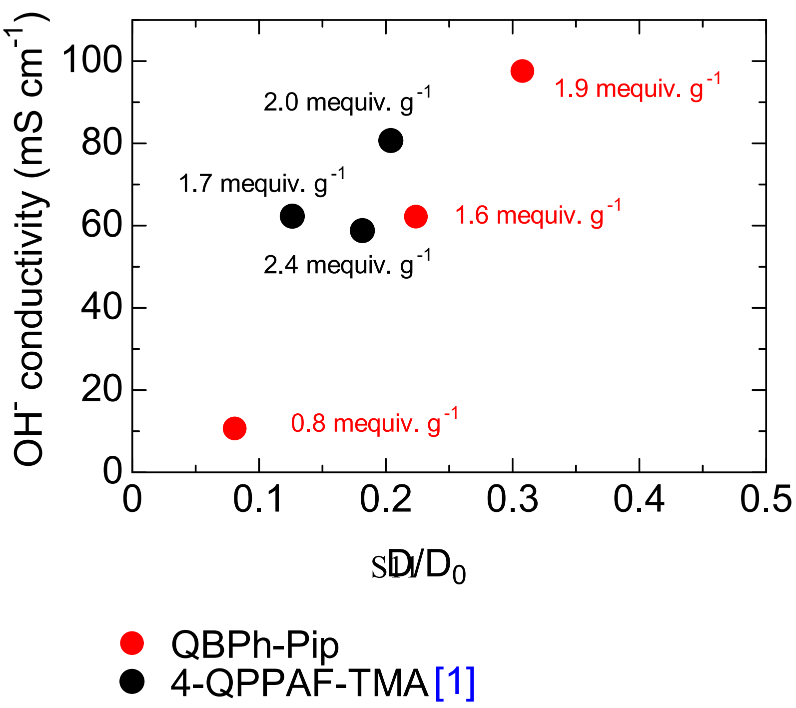

Fig. S12 Hydroxide ion conductivity of QBPh-Pip and 4-QPPAF-TMA membranes (adapted from ref. [1]) at 30 °C as a function of the normalized ion diffusion coefficient (D/D_0).

Table S1 Properties of post-test QBPh-Pip membranes.

IEC_{tit}[a] (mequiv. g^{-1})	Post-test IEC_{NMR}[b] (mequiv. g^{-1})	Post-test IEC_{tit} (mequiv. g^{-1})	Initial conductivity (mS cm^{-1})	Remaining conductivity (mS cm^{-1})
0.80	0.68	0.54	16.70	10.40
1.60	1.47	1.43	140.00	120.00
1.90	1.80	1.78	160.00	146.00

a) Estimated from Mohr titration method. b) determined from NMR integral ratios.

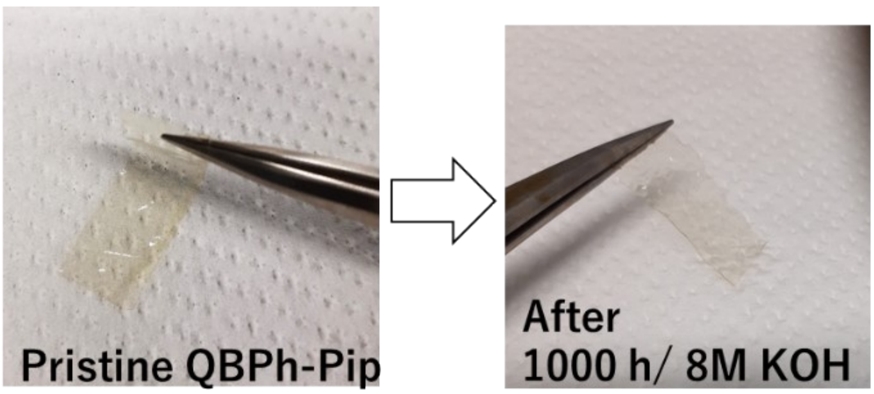

Fig. S13 Images of pristine and post-test QBPh-Pip membranes after 1,000 h in 8M KOH at 80 °C.

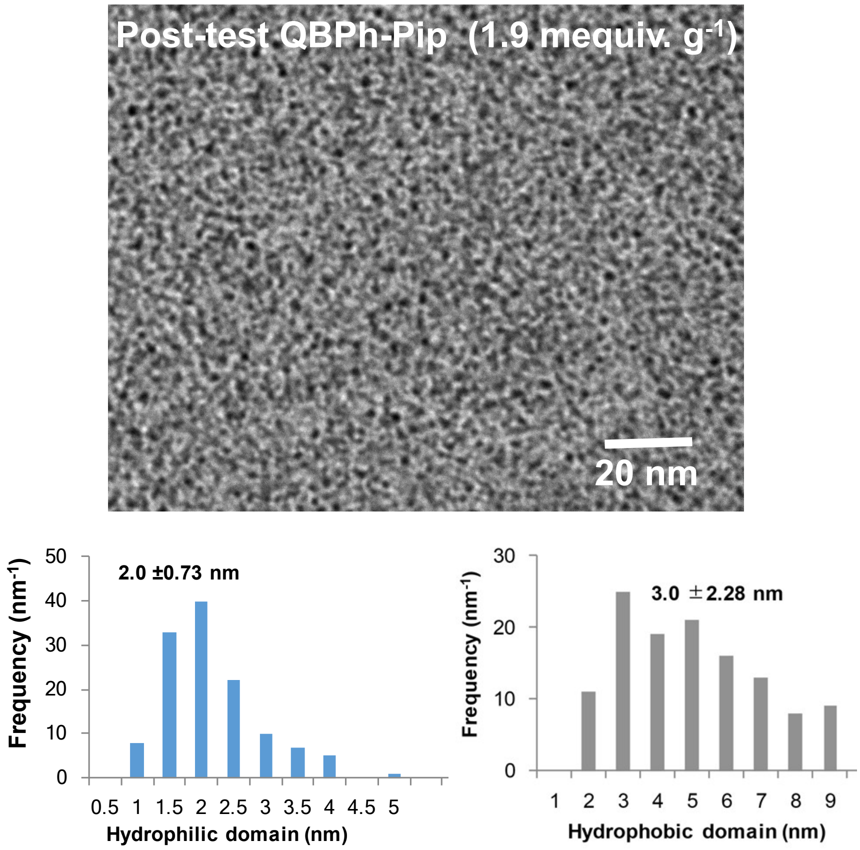

Fig. S14 Post-test TEM images of QBPh-Pip (IEC = 1.9 mequiv. g^{-1}) membrane after 1,000 h in 8M KOH at 80 °C.

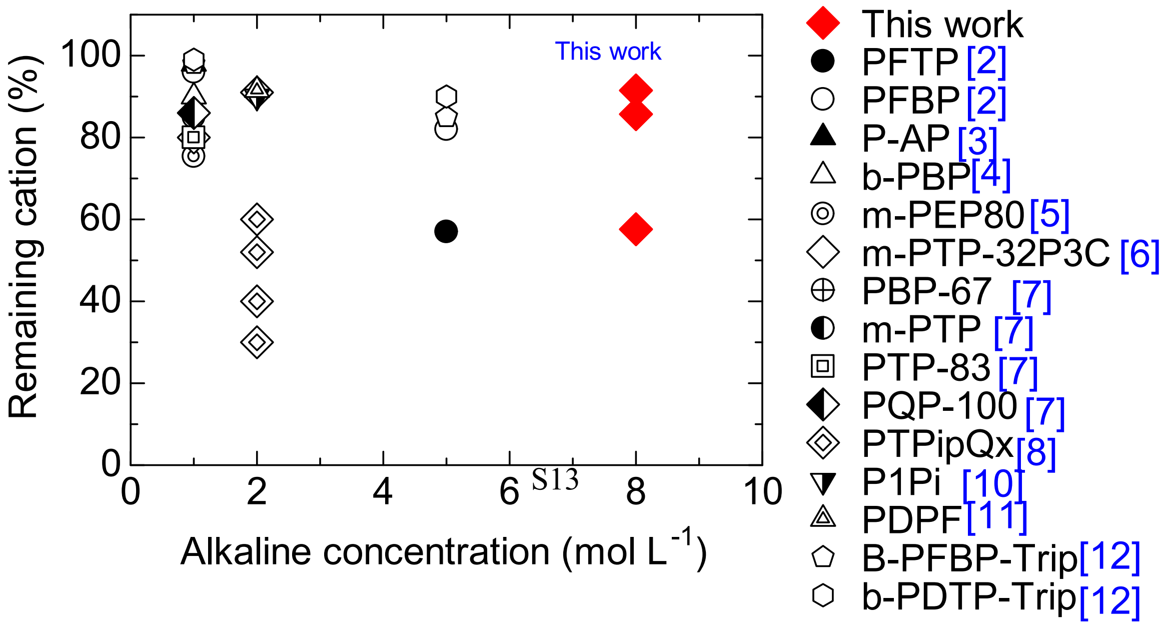

Fig. S15 Alkaline stability of QBPh-Pip and some other reported AEMs as a function of the alkaline concentration (mol L^{-1}).

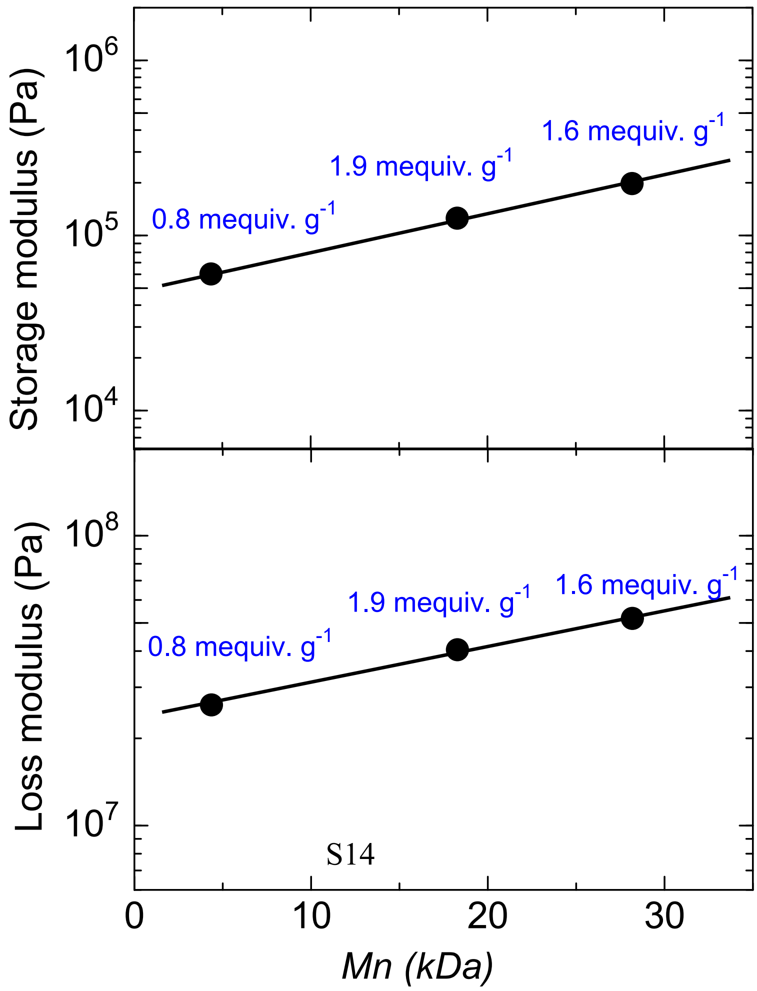

Fig. S16 Storage modulus and loss modulus of QBPh-Pip membranes as a function of number average molecular weight (M_n).

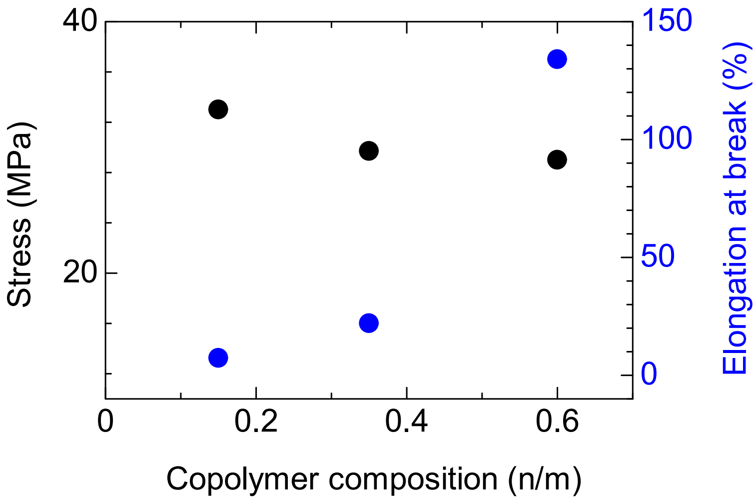

Fig. S17 The maximum stress and elongation at break (%) of QBPh-Pip membranes as a function of copolymer composition (n/m). where n/m represent the ratio between DPF to biphenyl.

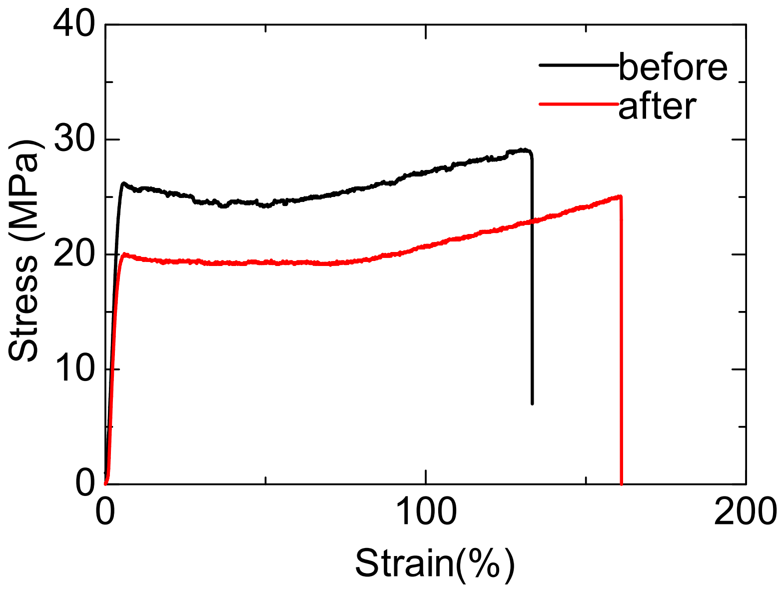

Fig. S18 Post-test stress-strain curve of QBPh-Pip (1.9 mequiv. g^{-1}) at 60%RH and 80 °C.

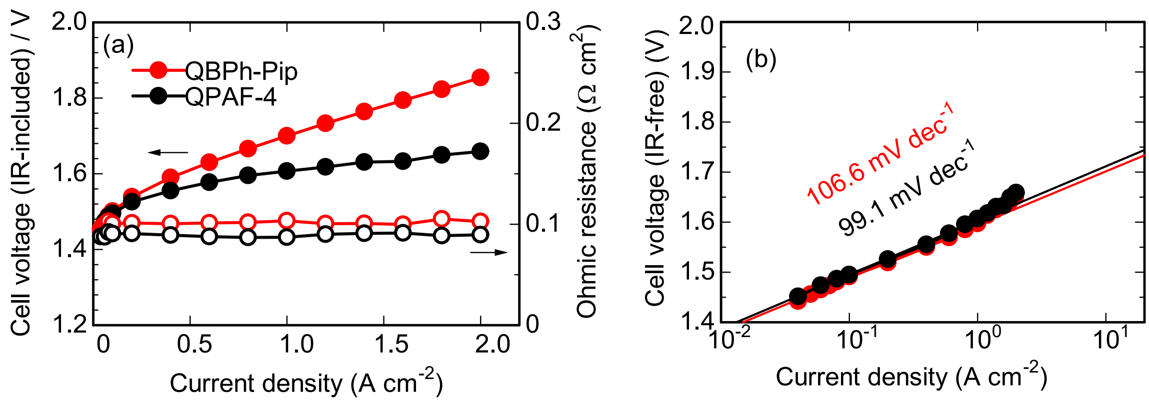

Fig. S19 **(a)** IR-included I-V curves and ohmic resistances, (b) IR-free Tafel plots of QBPh-Pip (1.9 mequiv. g^{-1}) cell with NiFeO anode and QPAF-4 (1.5 mequiv. g^{-1}) cell with NiCoO anode at 80 °C and 1 M KOH aqueous solution. (data of QPAF-4 cell was adapted from ref. [13])

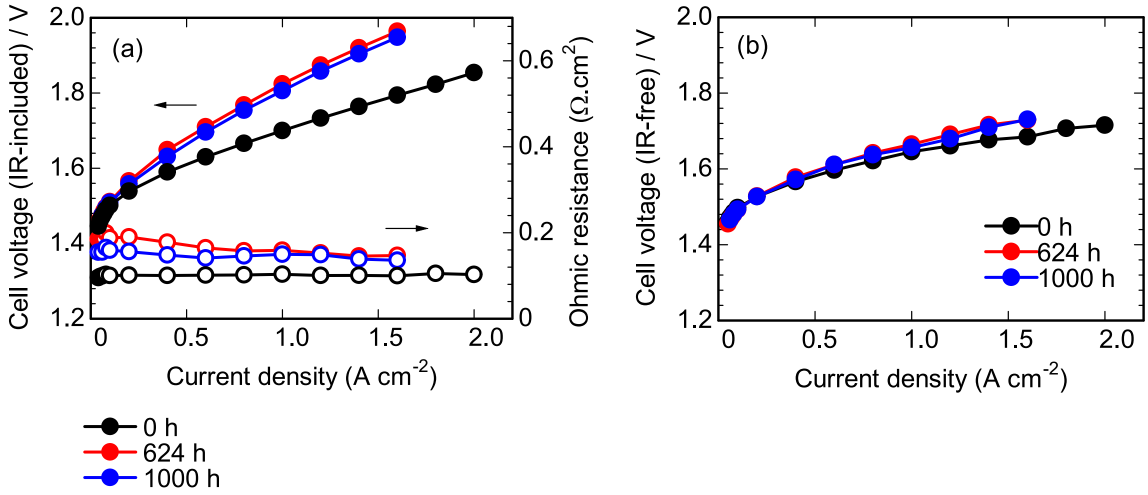

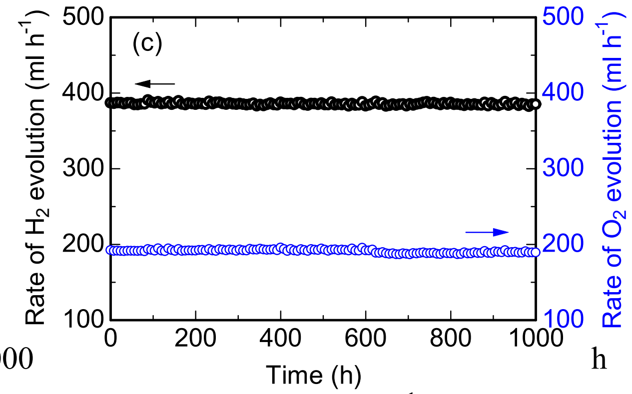

Figure S20 (a) IR-included IV curves and ohmic resistance, (b) IR-free I-V curves of QBPh-Pip (1.9 mequiv. g^{-1}) cell at 80 ℃ with 1 M KOH aqueous solution at 0 h, 624 h and 1000 h during the durability test. (c) Rate of H_2 and O_2 evolution (mL h^{-1}) as a function of the testing time.

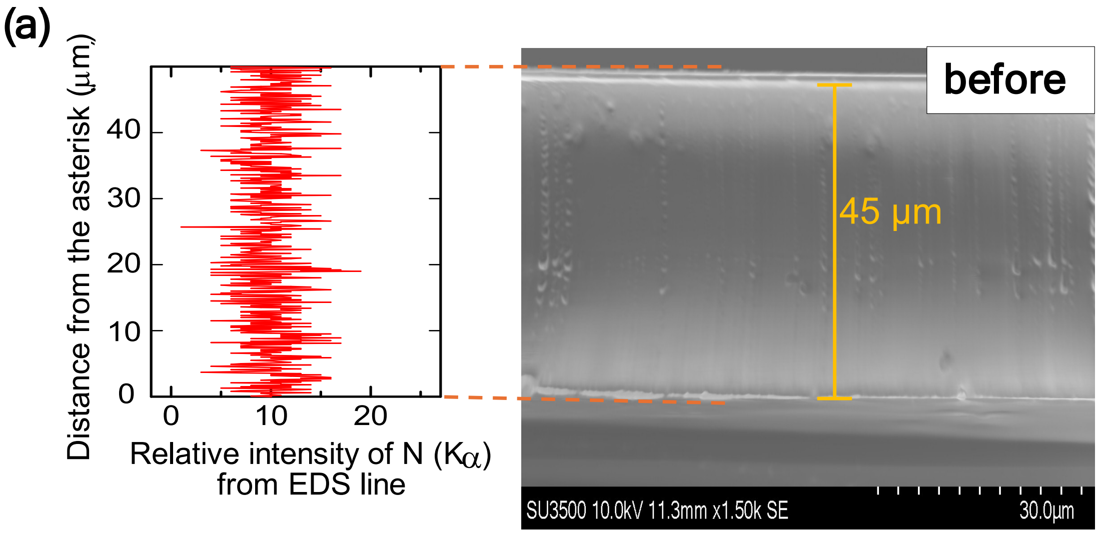

(a)
Distance from the asterisk (μm)
40
30
20
10
0
0
10
20
Relative intensity of N (Kα)
from EDS line
before
45 μm
SU3500 10.0kV 11.3mm x1.50k SE
30.0μm

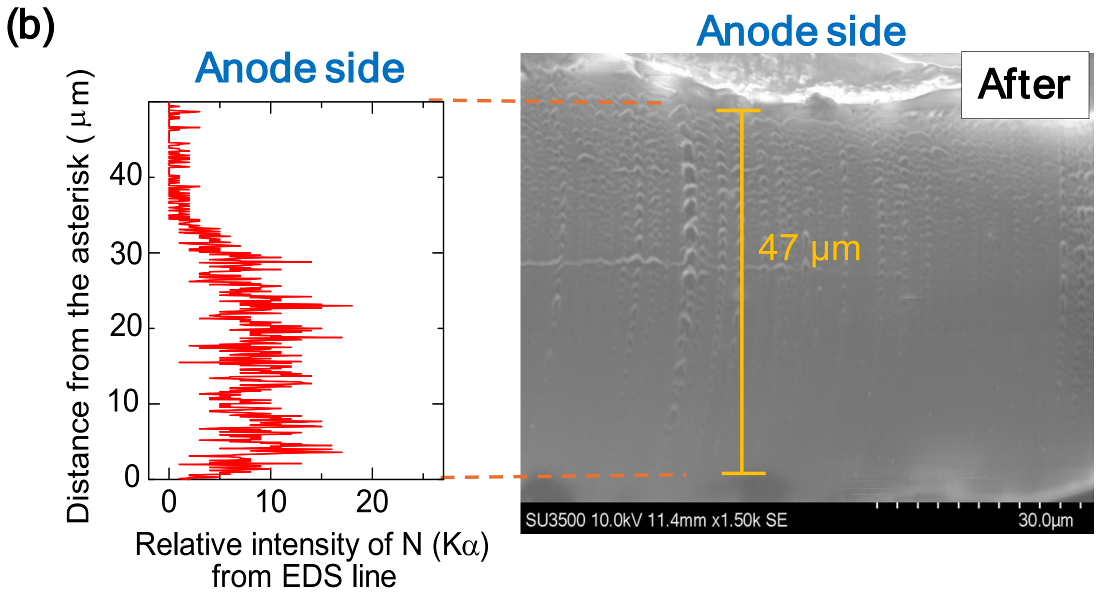

(b)
Anode side
Distance from the asterisk (μm)
40
30
20
10
0
0
10
20
Relative intensity of N (Kα)
from EDS line
Anode side
After
47 μm
SU3500 10.0kV 11.4mm x1.50k SE
30.0μm

Figure S21 Cross-sectional SEM images fitted with N atom (Kα) intensity on the EDS line analysis quantified by backscattered electrons as a function of the distance from the asterisk (μm) of QBPh-Pip (1.9 mequiv. g^{-1}), (a) before and (b) after 1000 h of durability test**.**

Table S2 Comparison of the AEM-WE performance of QBPh-Pip and reported AEM-WEs.

entry	AEM	Test condition	Anode	Cathode	Performance @ 1.0 A cm^{-2}	Durability	Rate of voltage increase	Ref.
1	QBPh-Pip	80 ℃, 1M KOH	NiFeCo (2.0 mg cm^{-2})	Pt/C (1.0 mg cm^{-2})	1.70 V	1000h@ 1.0 A cm^{-2}, 80℃	70 μV h^{-1}	This work
2	SustanionXA-9	80 ℃, 1M KOH	Ni-FeOOH/Ni foam (1.2 mg cm^{-2})	Pt/C (0.6 mg cm^{-2})	1.69 V	NA	NA	[3]
3	Aemion+	80 ℃, 1M KOH	Ni-FeOOH/Ni foam (1.2 mg cm^{-2})	Pt/C (0.6 mg cm^{-2})	1.70 V	NA	NA	[3]
4	Fumion	80 ℃, 1M	Ni-	Pt/C (0.6	1.69 V	NA	NA	[3]

		KOH	FeOOH/Ni foam (1.2 mg cm^{-2})	mg cm^{-2})				
5	PAP-TP-85	80 °C, KOH	Fe-NiOOH-20F	Pt/C (1.0 mg cm^{-2})	1.90 V	160 h @ 0.5 A cm^{-2}, 60°C	560 µV h^{-1}	[14]
6	FAA-3-50	80 °C, 1M KOH	Ni(Fe)OH (3.36 mg cm^{-2})	Pt/C (3.4 mg cm^{-2})	1.80 V	1300 h @ 2.0 Ac m^{-2}, 50 °C	180 µV h^{-1}	[15]
7	Sustanion X37-50	60 °C, 1M KOH	NiFe (2.5 mg cm^{-2})	Pt/C (1.0 mg cm^{-2})	1.78 V	500 h, (1-1.8V durability cycle), 25 °C	3820 µA cm^{-2} h^{-1}	[16]
8	Fumasep® FAA3-50	60 °C, 1M KOH	$NiFe_2O_4$ (3.0 mg cm^{-2})	Pt/C (0.5 mg cm^{-2})	1.76 V	120 h @ 2.0 V, 60 °C	1477 µA cm^{-2} h^{-1}	[17]
9	FAA-3-50	70 °C, 1M KOH	IrO_2 (4.0 mg cm^{-2})	Pt/C (0.4 mg cm^{-2})	1.77 V	NA	NA	[18]
10	FAA-3-50	70 °C, 1M KOH	IrO_2 (2.0 mg cm^{-2})	Pt/C (0.4 mg cm^{-2})	2.00 V	4.2 h @ 0.2 A cm^{-2}, 70 °C	48300 µV h^{-1}	[19]
11	PFPB-QA	70 °C, 1M KOH	IrO_2 (2.0 mg cm^{-2})	Pt/C (0.4 mg cm^{-2})	1.84 V	4.2 h @ 0.2 A cm^{-2}, 70 °C	32380 µV h^{-1}	[19]

References

1 A. M. A. Mahmoud and K. Miyatake, *ACS Appl. Polym. Mater.,* 2023, **5**, 2243–2253.

2 N. Chen, H. H. Wang, S. P. Kim, H. M. Kim, W. H. Lee, C. Hu, J. Y. Bae, E. S. Sim, Y. -C. Chung, J. -H. Jang, S. J. Yoo, Y. Zhuang and Y. M. Lee, *Nat. Commun.,* 2021, **12**, 2367.

3 N. Chen, Q. Jiang, F. Song and X. Hu, *ACS Energy Lett.,* 2023, **8**, 4043–4051.

4 X. Wu, N. Chen, H. A. Klok, Y. M. Lee and X. Hu, *Angew. Chem. Int. Ed*., 2022, **61**, e20211489.

5 H. Chen, K.-T. Bang, Y. Tian, C. Hu, R. Tao, Y. Yuan, R. Wang, D.-M. Shin, M. Shao, Y. M. Lee and Y. Kim, *Angew. Chem. Int. Ed.,* 2023, **62**, e202307690.

6 L. Xu, H. Wang, L. Min, W. Xu, Y. Wang and W. Zhang, *Ind. Eng. Chem. Res*., 2022, **61**, 14232–14241.

7 M. Liu, X. Hu, B. Hu, L. Liu and N. Li, *J. Membr. Sci.,* 2022, **642**, 119966.

8 J. S. Olsson, T. H. Pham and P. Jannasch, *Adv. Funct. Mater.,* 2018, **28**, 1702758.

9 T. H. Pham, J. S. Olsson and P. Jannasch, *J. Mater. Chem. A*, 2018, **6**, 16537-16547.

10 T. H. Pham, J. S. Olsson and P. Jannasch, *J. Mater. Chem. A*, 2019, **7**, 15895-15906.

11 T. H. Pham, A. Allushi, J. S. Olsson and P. Jannasch, *Polym. Chem.,* 2020, **11**, 6953-6963.

12 C. Hu, N. Y. Kang, H. W. Kang, J. Y. Lee, X. Zhang, Y. J. Lee, S.W. Jung, J. H. Park, M.-G. Kim, S. J. Yoo, S.Y. Lee, C. H. Park and Y. M. Lee, *Angew. Chem. Int. Ed.,* 2024, **63**, e2023166.

13 F. Liu, K. Miyatake, M. Tanabe, A. M. A. Mahmoud, V. Yadav, L. Guo, C.Y. Wong, F.

Xian, T. Iwataki, M. Uchida and K. Kakinuma, *Adv. Sci.,* 2024, **11**, 29, 2402969.

14 J. Xiao, A. M. Oliveira, L. Wang, Y. Zhao, T. Wang, J. Wang, B. P. Setzler and Y. Yan, *ACS Catal.,* 2020, **11**, 264.

15 J. Wang, C. Liang, X. Ma, P. Liu, W. Pan, H. Zhu, Z. Guo, Y. Sui, H. Liu, L. Liu and C. Yang, *Adv. Mater.,* 2023, **36**, 2307925.

16 S.C. Zignani, M. L. Faro, S. Trocino and A. S. Aricò, *Energies,* 2020, **13**, 1720.

17 A. Caprì, I. Gatto, C. L. Vecchio, S. Trocino, A. Carbone and V. Baglio, *ChemElectroChem,* 2023, **10**, e202201056.

18 J. E. Park, S. Y. Kang, S. H. Oh, J. K. Kim, M. S. Lim, C. Y. Ahn, Y. H. Cho and Y. E. Sung, *Electrochim. Acta,* 2019, ***295***, 99-106.

19 H. Lim, I. Jeong, J. Choi, G. Shin, J. Kim, T. H. Kim and T. Park, *Appl. Surf. Sci.,* 2023, ***610***, 155601.